Role of Glycosyltransferases in Pollen Wall Primexine Formation and Exine Patterning[1][OPEN]

Wenhua L. Li, Yuanyuan Liu, and Carl J. Douglas*

Department of Botany, University of British Columbia, Vancouver, British Columbia, Canada V6T 1Z4

ORCID ID: 0000-0001-8547-1589 (C.J.D.).

The pollen cell wall is important for protection of male sperm from physical stresses and consists of an inner gametophyte-derived intine layer and a sporophyte-derived exine layer. The polymeric constituents of the robust exine are termed sporopollenin. The mechanisms by which sporopollenin is anchored onto microspores and polymerized in specific patterns are unknown, but the primexine, a transient cell wall matrix formed on the surface of microspores at the late tetrad stage, is hypothesized to play a key role. Arabidopsis (*Arabidopsis thaliana*) *spongy* (*spg*) and *uneven pattern of exine* (*upex*) mutants exhibit defective and irregular exine patterns. *SPG2* (synonymous with *IRREGULAR XYLEM9-LIKE* [*IRX9L*]) encodes a family GT43 glycosyltransferase involved in xylan backbone biosynthesis, while *UPEX1* encodes a family GT31 glycosyltransferase likely involved in galactosylation of arabinogalactan proteins. Imaging of developing *irx9l* microspores showed that the earliest detectable defect was in primexine formation. Furthermore, wild-type microspores contained primexine-localized epitopes indicative of the presence of xylan, but these were absent in *irx9l*. These data, together with the *spg* phenotype of a mutant in *IRX14L*, which also plays a role in xylan backbone elongation, indicate the presence of xylan in pollen wall primexine, which plays a role in exine patterning on the microspore surface. We observed an aberrant primexine and irregular patterns of incipient sporopollenin deposition in *upex1*, suggesting that primexine-localized arabinogalactan proteins could play roles in sporopollenin adhesion and patterning early in microspore wall development. Our data provide new insights into the biochemical and functional properties of the primexine component of the microspore cell wall.

The development of a durable wall surrounding the angiosperm male gametophyte (pollen) is important for protection of the male sperm from physical stresses including abrasion, desiccation, and UV radiation. This protective wall is a complex extracellular matrix with an inner gametophyte-derived intine layer and a robust exine outer sporophyte-derived exine layer upon which a lipid-rich pollen coat, or tryphine, is deposited (Ariizumi and Toriyama, 2011; Quilichini et al., 2015a). The intine resembles the primary cellulosic plant cell wall (Ariizumi and Toriyama, 2011; Heslop-Harrison 1968a; Blackmore et al., 2007). The outer exine exhibits species-specific patterning. In Arabidopsis (*Arabidopsis thaliana*) and other plants, the exine is reticulate, composed of radially directed rods (baculae) and an end roof (tectum; Ariizumi and Toriyama, 2011; Quilichini et al., 2015a). The polymeric constituents of the exine are termed sporopollenin (Ariizumi and Toriyama, 2011; Quilichini et al., 2015a; Scott et al., 2004), which chemical evidence suggests is a heterogeneous polymer composed of polyhydroxylated aliphatic constituents with aromatic or conjugated side chains containing ether and ester bonds (Ahlers et al., 2000, 2003; Blokker et al., 2006; Bubert et al., 2002).

Sporopollenin precursors are synthesized in the tapetum, a metabolically active anther secretory tissue that surrounds the anther locule where microspores and pollen grains develop (Ariizumi and Toriyama, 2011; Quilichini et al., 2014a, 2015a). The morphological and cellular events involved in pollen and pollen wall development have been most thoroughly studied in Arabidopsis and rice (*Oryza sativa*; Sanders et al., 1999; Scott et al., 2004; Ariizumi and Toriyama, 2011; Shi et al., 2015). A recent detailed study of microspore and tapetum development over the course of Arabidopsis anther development has revealed the events in pollen wall formation at high resolution with greatly improved preservation of ultrastructural features (Quilichini et al., 2014a). Briefly, pollen wall formation is initiated after microspore mother cells undergo meiosis to generate haploid tetrads surrounded by callose. At the tetrad stage, a primexine layer, presumed to be polysaccharide based (Heslop-Harrison, 1968b; Ariizumi and Toriyama, 2011; Jiang et al., 2013; Shi et al., 2015), is synthesized and deposited on the outside of the microspore plasma

[1] This work was supported by Discovery Grant RGPIN 36485-12 from the Natural Sciences and Engineering Research Council of Canada to C.J.D.

* Address correspondence to carl.douglas@ubc.ca.

The author responsible for distribution of materials integral to the findings presented in this article in accordance with the policy described in the Instructions for Authors (www.plantphysiol.org) is: Carl J. Douglas (carl.douglas@ubc.ca).

C.J.D. conceived the original research plans and project and supervised the experiments; W.L.L. performed most of the experiments; Y.L. provided assistance for some experiments; W.L.L. and C.J.D. designed the experiments and analyzed the data; W.L.L. wrote a first draft of the article; C.J.D. supervised the writing and prepared the final draft of the article.

[OPEN] Articles can be viewed without a subscription.

www.plantphysiol.org/cgi/doi/10.1104/pp.16.00471

membrane inside the encasing callose. Recent data suggest that primexine is of sporophytic origin (Ariizumi and Toriyama, 2011), and it is observed transiently during pollen wall development (Blackmore et al., 2007; Ariizumi and Toriyama, 2011; Quilichini et al., 2014a). Shortly after the appearance of the primexine at the tetrad stage, incipient baculae (probaculae) appear within the primexine matrix, which is likely composed of sporopollenin (Quilichini et al., 2014a). After the tetrad stage, the callose wall degenerates, releasing free microspores into the locule. At this stage (early to late uninucleate free microspore stage), pollen wall development is characterized by rapid sporopollenin deposition and formation of a patterned exine structure consisting of baculae and tecta, and only remnants of the primexine are evident (Quilichini et al., 2014a). In parallel with free microspore release, deposition of a thin microspore-derived intine wall is evident, forming a layer between the microspore plasma membrane and the developing exine (Quilichini et al., 2014a). The final stages of anther development are dehiscence and the release of the mature pollen grains (Sanders et al., 1999; Scott et al., 2004).

Recent studies have shown that a major and critical event in exine formation and sporopollenin deposition is the biosynthesis of tetraketide-α-pyrones, via a genetically and biochemically defined metabolic pathway localized in tapetal cells (Morant et al., 2007; de Azevedo Souza et al., 2009; Dobritsa et al., 2009, 2010; Grienenberger et al., 2010; Kim et al., 2010; Lallemand et al., 2013). These polyketide sporopollenin precursors are secreted from tapetal cells by the action of the ATP binding cassette transporter ABCG26 (Quilichini et al., 2010, 2014b). Based on the coincidence of probaculae formation and primexine deposition, it is hypothesized that the primexine matrix plays a key role in providing a substrate for anchoring sporopollenin deposition on the microspore surface, and may play a role in exine patterning (Blackmore et al., 2007; Ariizumi and Toriyama, 2011; Quilichini et al., 2014a). However, the potential physical and biochemical interactions between incipient sporopollenin deposition in probaculae and the primexine are not understood.

Despite the hypothesized importance of the primexine in exine deposition and pattern determination, the composition of this scaffold layer and its biosynthetic origin are poorly understood. Chemical staining and treatment with cellulase suggest that, in *Lilium longiflorum*, this layer contains cellulose (Heslop-Harrison, 1968b). Genetic and biochemical approaches have failed, to date, to provide additional information on the specific chemical nature of the primexine or of the enzymes and metabolic pathways required for its formation. However, in support of a role for the primexine in exine deposition, several Arabidopsis mutants with altered exine deposition are defective in primexine formation, including *defective in exine formation1* (*dex1*), *ruptured pollen grain1* (*rpg1*), and *no exine formation1* (*nef1*; Paxson-Sowders et al., 2001; Guan et al., 2008; Ariizumi et al., 2004; Sun et al., 2013).

Identification of additional genes defective in exine patterning may provide a better understanding of primexine composition and structure, mechanisms underlying sporopollenin attachment to the microspore surface, and mechanisms underlying exine patterning. A large-scale genetic screen reported by Dobritsa et al. (2011) identified a number of exine-patterning mutants and identified two genes encoding glycosyltransferases (GTs) that are important for this process. The *uneven pattern of exine* (*upex*) pollen phenotype includes patches of missing exine and an exine layer that dissociates from the pollen surface more easily compared to wild type, leaving the pollen partially exine-less (Dobritsa et al., 2011). *UPEX1* (At1g33430) is coexpressed with genes in the sporopollenin synthesis pathway (de Azevedo Souza et al., 2009; Dobritsa et al., 2011; Grienenberger et al., 2010; Kim et al., 2010) and encodes a carbohydrate-active enzyme GT31 family protein (Campbell et al., 1997; Qu et al., 2008). UPEX1 is positioned in group A with Arabidopsis galactosyltransferase (GalT) proteins (Qu et al., 2008), some of which have been characterized as arabinogalactan protein (AGP) GalTs (Geshi et al., 2013; Ogawa-Ohnishi and Matsubayashi, 2015), suggesting that UPEX1 could have a similar GalT activity in AGP galactosylation.

The *spongy* (*spg*) pollen phenotype (Dobritsa et al., 2011) includes an irregular exine pattern lacking the regular net-like reticulate pattern of wild-type pollen, with tecta of variable sizes. *SPG2* (At1g27600) encodes the previously characterized IRREGULAR XYLEM9-LIKE (IRX9L) GT family 43 protein (Wu et al., 2010). *IRX9L* is a paralog of *IRX9*, required for β-1-4-xylan backbone elongation during hemicellulose glucuronoxylan (GX) biosynthesis (Peña et al., 2007). IRX9 and IRX9L proteins share 64% amino sequence, and IRX9L/SPG2 appears to have a similar biochemical function to IRX9 based on its high degree of similarity and the enhanced xylan deficient phenotype of *irx9 irx9l* double mutants (Wu et al., 2010).

Here, we tested the hypothesis that *UPEX1* and *IRX9L/SPG2* function in exine patterning in developing Arabidopsis microspores by modulating the synthesis or modification of components of the primexine wall layer. Detailed analysis of the *upex1* and *irx9l* mutant phenotypes over the course of anther development indicated that both mutants are defective in primexine formation at the early tetrad stage and that exine patterning defects are evident immediately thereafter. We used immunolabeling to show that xylan epitopes are present at the surface of developing microspores in wild-type anthers, suggesting that the primexine contains this polysaccharide. While *irx9l* mutants lack detectable xylan in the walls of developing microspores, *upex1* mutants exhibit enhanced cross reactivity to an antixylan antibody, suggesting a change in primexine cell wall structure with increased abundance or enhanced accessibility of the xylan epitope. Promoter-reporter gene assays and genetic analyses were consistent with functions of *UPEX1* and *IRX9L/SPG2* in sporophytic tapetal cells. These data support a model in which xylan and AGP cell wall components synthesized in the tapetum are incorporated into the

primexine wall and play roles in primexine development and anchoring of sporopollenin to the microspore surface early in microspore development.

RESULTS

Loss-of-Function Alleles of GTs At1g33430 and At1g27600

A large-scale screen for Arabidopsis mutants affecting pollen exine formation identified *UPEX1* (At1g33430) and *SPG2/IRX9L* (At1g27600) as Arabidopsis genes encoding GTs involved in exine patterning (Dobritsa et al., 2011). We obtained the previously identified *irx9l-1* loss-of-function T-DNA insertion allele (Salk_037323; Wu et al., 2010), and two previously described *upex1* T-DNA insertion alleles (Salk_091466 insertion in exon 1; Sail_544-C02, insertion in exon 3; Dobritsa et al., 2011), which we renamed *upex1-1* and *upex1-2*, respectively. Homozygous plants were identified by PCR-aided genotyping, and reverse transcription PCR (RT-PCR) with template cDNA derived from mutant flower buds confirmed that *irx9l-1* and *upex1-1* lack wild-type transcripts and are loss-of-function alleles, and that *UPEX1* has a flower-specific expression pattern (Supplemental Figs. S1 and S2). Two *UPEX1* transcripts, *UPEX1.1* and *UPEX1.2*, are annotated as having alternative 5′ splice acceptor sites (The Arabidopsis Information Resource, http://www.arabidopsis.org/). RT-PCR with variant-specific primers and cDNA template derived from wild-type flower buds showed that the major variant is the shorter transcript, *UPEX1.1* (Supplemental Fig. S3). The *irx9l-1* and *upex1-1* alleles were used for all subsequent analyses. Homozygous *irx9l* and *upex1* plants grew normally (Supplemental Figs. S1 and S2) and showed no reductions in fertility (Supplemental Table S1).

We initially analyzed *irx9l* and *upex1* pollen phenotypes by staining mature pollen grains with Auramine O and viewing them with fluorescence microscopy (Grienenberger et al., 2010; Kim et al., 2010; Dobritsa et al., 2011) to reveal any differences in exine structure and patterning. Using this method, *irx9l* was found to produce pollen without the regular reticulate and net-like exine pattern typical of wild-type pollen (Fig. 1). This confirms the *spg* phenotype of *irx9l* pollen reported by Dobritsa et al. (2011). Light microscopy of toluidine blue-stained wild-type and *irx9l* microspores at the free microspore stage after exine deposition (Fig. 1) indicated that the *irx9l* microspores had similar morphology to wild type at this stage. We also imaged *irx9l* pollen using two-photon (2P) microscopy, which allows live cell imaging of microspores in intact anthers using the intrinsic autofluorescence of exine under UV excitation (Quilichini et al., 2014b, 2015b). As seen in Figure 1, *irx9l* microspores appeared to have a thinner pollen wall compared to wild type with less intense emission, but the exine showed similar autofluorescence. No changes in the autofluorescence of tapetal cells or the locular matrix were observed.

We carried out similar investigations of *upex1* pollen phenotypes relative to wild type. Mature pollen from *upex1-2* had the same phenotypes as *upex1-1* by Auramine O staining, and all further experiments were carried out using *upex1-1.* Auramine-O-stained *upex1* pollen had sporopollenin/exine-like material anchored to the microspore in patches, with areas of reticulated exine missing and some material apparently loosely attached (Fig. 1). This confirms the *upex1* phenotype reported by Dobritsa et al. (2011). Toluidine-blue-stained *upex1* mutant anther sections consistently showed irregularly shaped microspores with apparently unanchored exine-like material in the locule, and

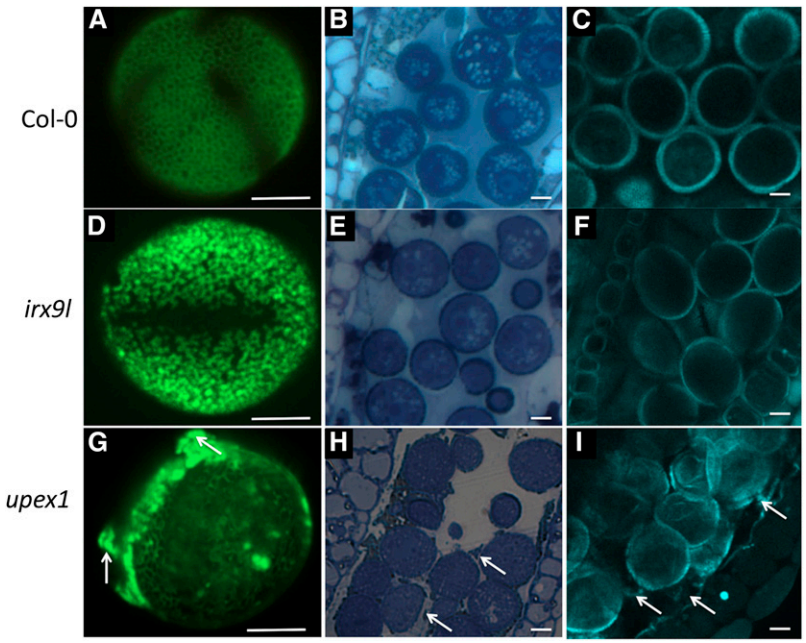

Figure 1. *irx9l* and *upex1* pollen phenotypes. A to C, Wild-type pollen; D to F, *irx9l* pollen; G to I, *upex1* pollen. A, C, and D, Auramine-O-stained mature pollen released from anthers viewed by fluorescence microscopy. B, E, and H, Light micrographs of images of chemically fixed 12-μm sections from late free microspore stage anthers stained with toluidine blue. C, F, and I, 2P micrographs of intact late free microspore stage anthers with excitation at 640 nm. E and F, *irx9l* pollen appears to have thinner pollen wall compared to wild-type pollen. Arrows indicate sporopollenin-like exine components apparently unanchored to *upex1* microspores. Scale bars = 5 μm.

2P microscopy imaging of the locules of *upex1* anthers also revealed irregularly shaped microspores (Fig. 1). While autofluorescent exine was present, the fluorescence was more diffuse than in wild type, and autofluorescent accumulations in the locules, apparently unanchored to the developing microspores, were observed. Such accumulations were never seen in images of wild-type anthers (Fig. 1).

Phenotypic Analysis of *irx9l* and *upex1* Pollen by Scanning Electron Microscopy

We used scanning electron microscopy (SEM) to provide greater resolution of pollen grain surfaces and to reveal the extent of exine-patterning phenotypes. Compared to wild-type pollen, mature *irx9l* pollen had a *spg* exine appearance, and pollen grains appeared collapsed (Fig. 2). To test if the collapsed phenotype was the result of the vacuum used during SEM sample processing or if the pollen grains were naturally collapsed, we used cryo-SEM. As seen in Figure 2, the collapsed pollen grain phenotype was no longer present in these samples relative to wild type, suggesting that the *irx9l* collapsed pollen phenotype is likely the result of a weaker pollen wall that is unable to maintain its structural integrity under a vacuum. Likewise, SEM confirmed the *upex1* phenotype of patchy and uneven exine deposition and also showed that the pollen grains were collapsed, which has not been described previously (Fig. 2).

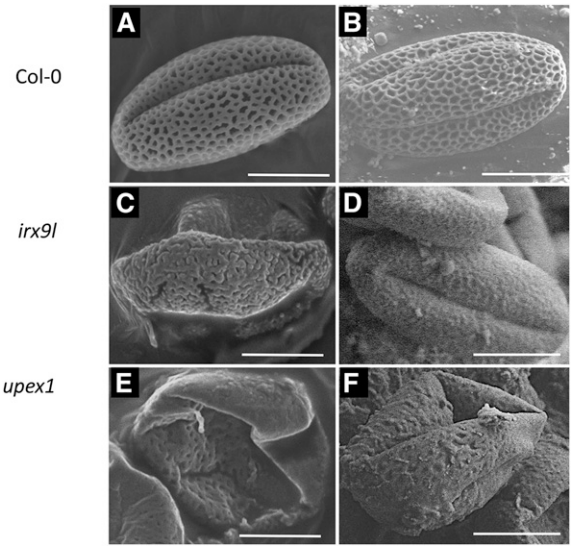

Figure 2. Pollen phenotype analyses using scanning electron microscopy. A and B, Wild type; C and D, *irx9l*; E and F, *upex1*. A, C, and E, SEM micrographs; B, D, and F, cyro-SEM micrographs. C, *irx9l* pollen appears to have *spg* exine and is collapsed compared to wild type. D, Cryofixed *irx9l* pollen appeared to have *spg* exine and a regular cell shape compared to wild type. E, *upex1* pollen appears to have patches of exine missing and is collapsed compared to wild type. F, Cryofixed *upex1* pollen appears collapsed with patches of exine missing. Scale bars = 10 μm.

upex1 pollen grains were still collapsed relative to normal appearing wild-type pollen grains in cryo-SEM (Fig. 2), indicating that the collapsed phenotype is the natural state of some of *upex1* pollen grains. This further confirms the presence of naturally collapsed pollen grains in *upex1* as seen by 2P imaging (Fig. 1).

Light and Transmission Electron Microscopy Characterization of Anther and Microspore Development in Wild-Type, *irx9l*, and *upex1* Flowers

We used light microscopy of anther cross sections at microspore and pollen developmental stages as defined by Quilichini et al. (2014a) to compare anther development in wild type (Col-0) and the two mutants to establish the timing of the onset of their phenotypes. In *irx9l* anthers, microspore development appeared similar to wild type in the microspore mother cell and tetrad stages (Fig. 3). At the late uninucleate microspore stage when sporopollenin deposition/accumulation was evident in the free microspores, *irx9l* microspore walls appeared to be less reticulate and amorphous compared to wild type (Fig. 3). This was less evident in maturing microspores at the bicellular free microspore stage, and mature *irx9l* pollen grains appeared relatively normal (Fig. 3).

In *upex1* anthers, microspores also appeared to be similar to wild type in early stages of microspore development (Fig. 3). At the late uninucleate stage, *upex1* microspores appeared to adhere together and to have a poorly developed exine, unlike wild-type microspores. In maturing pollen, *upex1* microspores were misshapen and had an unevenly distributed exine relative to wild type, and we observed debris in the locules that was not anchored to the microspores (Fig. 3).

We next used transmission electron microscopy (TEM) to examine microspore wall development at higher resolution in *irx9l* and *upex1* plants. As seen in Figure 4, wild-type microspores had a uniform primexine matrix surrounding each microspore, within the callose layer, at early tetrad stage. At late tetrad stage, electron-dense materials were deposited onto the primexine next to the callose, and these electron-dense materials in the primexine matrix then elongated and appeared connected to the microspore plasma membrane (Fig. 4). These events observed in wild-type plants are consistent with those observed in a detailed analysis of Arabidopsis microspore development (Quilichini et al., 2014a). Compared to wild type, the primexine layer surrounding *irx9l* microspores was much thinner at early tetrad stage (Fig. 4). On the other hand, the primexine matrix surrounding the *upex1* microspore appeared to be less compact and was irregular in width. Exine formation initiated with the formation of the probaculae following the early tetrad stage. However, in contrast to the uniform and regular probaculae in wild type, *irx9l* microspores developed these electron-dense probaculae in a less uniform manner, and the electron-dense probaculae that formed within the primexine layer surrounding *upex1* microspores were ill defined and diffuse (Fig. 4). In contrast to wild-type microspores with

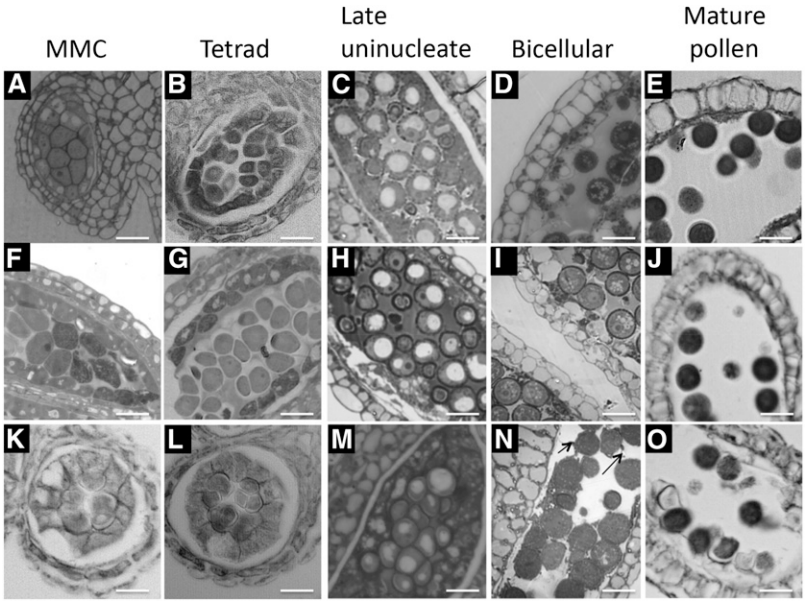

Figure 3. Phenotypic characterization of anther and microspore development in wild-type Col-0, *irx9l*, and *upex1* flowers. Light micrographs of wild-type and mutant anthers at different stages of development are shown. A to E, Wild-type (Col-0); F to J, *irx9l*; K to O, *upex1*. A, F, and K, Microspore mother cell (MMC) stage anthers. B, G, and L, Tetrad stage anthers. C, H, and M, Late uninucleate microspore stage anthers. D, I, and N, Bicellular free microspore stage anthers. E, J, and O, Dehiscent stage anthers. Anther/microspore development in the *irx9l* mutant appeared similar to wild type until the late uninucleate microspore stage when exine is evident in the free microspores. *irx9l* pollen appeared to have a thinner and less reticulate wall compared to wild type at the bicellular stage, but mature pollen appeared relatively normal. The microspore development defect in *upex1* was clearly visible at the late uninucleate microspore stage, when *upex1* microspores do not separate from each as in wild type. At later stages, *upex1* microspores and pollen were irregularly shaped with apparent unanchored exine visible at the bicellular free microspore stage (arrows, N). Scale bars = 25 μm.

probaculae that became elongated to form baculae with uniform width, *irx9l* probaculae were variable in width (Fig. 4) and became elongated to form baculae with nonuniform width at apparently higher density as development proceeded in *irx9l* pollen. Compared to wild type, the electron-dense probaculae that formed within the primexine layer surrounding *upex1* microspores appeared ill defined and diffuse (Fig. 4). As development proceeded, the baculae that formed in the *upex1* mutant were irregular in size and shape at the early unicellular microspore stage (Fig. 4). By the middle to late unicellular microspore stage, *upex1* mutant microspores lacked the reticulate exine pattern seen in wild type and had exine irregularly deposited on microspore surface, and unanchored exine-like compounds were visible in the locule (Fig. 4). These results indicate that the first observable differences in microspore development between *irl9l* and *upex1* mutants and wild type are defects in primexine development observed at the early tetrad stage, which are correlated with defective exine phenotypes observed later in microspore development.

Immunolocalization of Xylan during Wild-Type and Mutant Microspore Development

Since both IRX9 and IRX9L are involved in the synthesis of the hemicellulose xylan backbone in Arabidopsis secondary cell walls (Wu et al., 2010), we used the xylan-specific antibody LM10 to determine if xylan is present in the walls of developing microspore sections taken from wild-type and mutant anthers. Figure 5 shows that LM10-treated wild-type sections taken from anthers at the uninucleate ring-vacuolate free microspore stage (Quilichini et al., 2014a) had LM10-specific fluorescence surrounding most of the microspores while this signal was not observed in the *irx9l* mutant sample. No fluorescence signal was observed in samples processed without LM10 (Fig. 5). This indicates that xylan is present in the free microspore wall, and that IRX9L activity is required for its proper exine formation. In *upex1* anthers, an LM10 signal similar in intensity to wild type was observed and was absent in the control not treated with LM10 (Fig. 5). This suggests that normal levels of xylan are present in the *upex1* microspores, despite the patchy exine and uneven primexine observed in this mutant (Fig. 4)

We next used LM10 to determine if xylan could be detected in microspore walls as early as the tetrad stage, when the primexine layer is formed. As shown in Figure 6, no signal was found in wild-type or *irx9l* anthers at this stage. However, surprisingly, *upex1* anthers at the same stage showed a clear LM10-specific fluorescence signal surrounding each developing microspore, indicating the presence of xylan in the *upex1* microspore

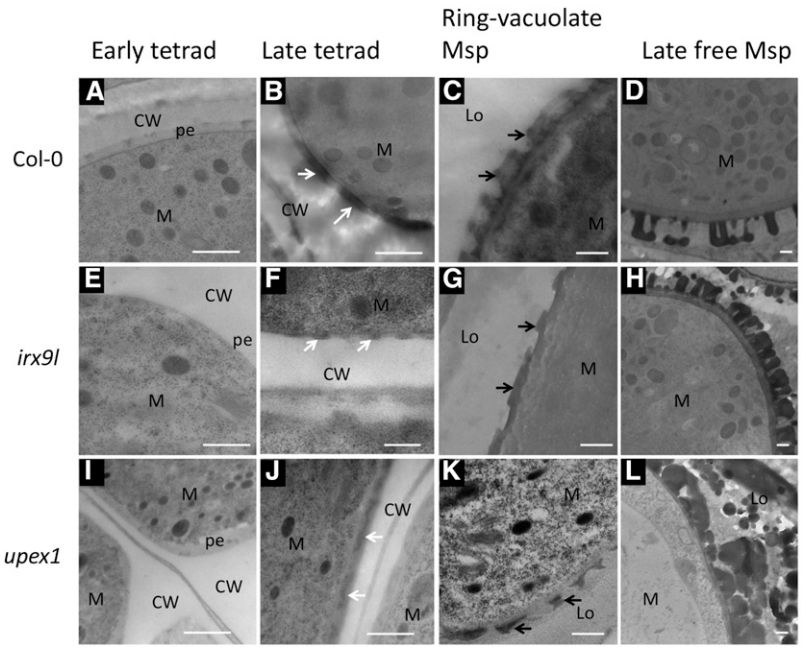

Figure 4. Transmission electron micrographs of wild-type Col-0, *irx9*, and *upex1* microspore development. Wild-type (Col-0), *irx9l*, and *upex1* samples were prepared in parallel by high-pressure freezing of anthers taken at developmental stages as defined by Quilichini et al. (2014a). A to D, Wild type; E to H, *irx9l*; I to L, *upex1*. A, E, and I, Early tetrad stage microspores; B, F, and J, late tetrad stage microspores; C, G, and K, ring-vacuolate stage microspores; D, H, and L, late free microspore stage. A, Primexine was deposited between the plasma membrane of the microspore and the inner callose wall in wild-type microspores at the early tetrad stage. E, *irx9l* showed a thinner primexine layer compared to wild type at the early tetrad stage. F, *irx9l* microspores showed uneven probaculae formation relative to wild type. G, Unevenly thickened baculae in *irx9l* are evident. I, *upex1* has nonuniform width primexine layer compared to wild type (A). J, Irregular probaculae formation in *upex1*. K, Irregularly sized baculae in *upex1*. In B, F, and J, white arrows indicate probaculae. In C, G, and K, black arrows indicate baculae. CW, Callose; pe, primexine; Lo, locule; M, microspore. Scale bars = 500 nm.

at the tetrad stage. No signal was seen in sections processed without LM10 (Fig. 6).

Finally, we examined sections taken from wild-type and mutant anthers at the early free microspore stage (Quilichini et al., 2014a), just after the tetrad stage and earlier than the ring-vacuolate stage shown in Figure 5, for the presence of detectable xylan. Wild-type samples showed weak but detectable LM10-derived fluorescence signal surrounding microspores, while such fluorescence was not observed in *irx9l* samples at a similar stage or in samples processed in the absence of LM10 (Fig. 7). In *upex1* mutant samples at this stage, the LM10 signal surrounding each microspore was readily detectable, and appeared to be stronger than in wild type (Fig. 7).

TEM Immunogold Localization of Xylan Epitopes in Developing Microspores

In order to determine at the ultrastructural level the location of the xylan epitopes responsible for the fluorescence seen using light microscopy, we performed immunogold labeling coupled with TEM using sections take from wild-type, *irx9l*, and *upex1* anthers at tetrad, early unicellular microspore and ring-vacuolate free microspore developmental stages. No immunogold labeling signal was detected in wild-type samples at the tetrad stage, consistent with the light microscopy immunolabeling data (Fig. 8). However, positive immunogold labeling was observed in the *upex1* anthers at this stage, where it appeared to be localized to the primexine layer (Fig. 8), again consistent with the immunofluorescence data. No signal was observed in *upex1*samples at this stage processed without LM10 (Fig. 8).

At the early uninucleate microspore stage, in which wild-type microspores had a well-defined primexine and incipient probaculae, significant immunogold labeling was observed specifically on the primexine layer (Fig. 9). These data are consistent with immunolabeling of wild-type microspores at the early unicellular microspore stage using light microscopy (Fig. 7). In the *upex1* mutant, the immunogold signal that appeared somewhat stronger than in wild type was also detected in the primexine layer, while labeling was not found in the *irx9l* mutant sample of the same stage (Fig. 9).

We also examined unicellular microspores at a later stage in development (miduninucleate stage), in which the exine was further developed. As seen in Figure 10, wild-type and *upex1* microspores both showed positive LM10 labeling in areas surrounding the exine baculae and tecta. However, immunogold signals were absent in *irx9l* microspores of at a similar stage (Fig. 10). Taken together with LM10 immunofluorescence data on wild-type and *upex1* anthers, these immunogold labeling results confirm that xylan is present in the primexine of *upex1* at the tetrad stage and in the primexine of wild-type and *upex1* at the early unicellular microspore stage and remains as a wall constituent over the course of exine deposition. With respect to xylan, the *upex1* microspore wall is distinguished from wild-type walls by an apparent higher LM10 signal, based on immunogold labeling. To quantify this, we counted gold particles in LM10 immunogold-labeled TEM sections taken from wild-type, *upex*, and *irx9l* early uninucleate stage anthers. Supplemental Figure S4 indicates that there was a significant in increase xylan signal (no. of gold particles per sample) in *upex1* compared to wild-type anthers, and almost no signal from *irx9l* anthers.

IRX9L and *UPEX1* Expression

IRX9L is expressed in multiple cell types and tissues in Arabidopsis stems and leaves (Wu et al., 2010). In order to determine the cell types in which the gene is

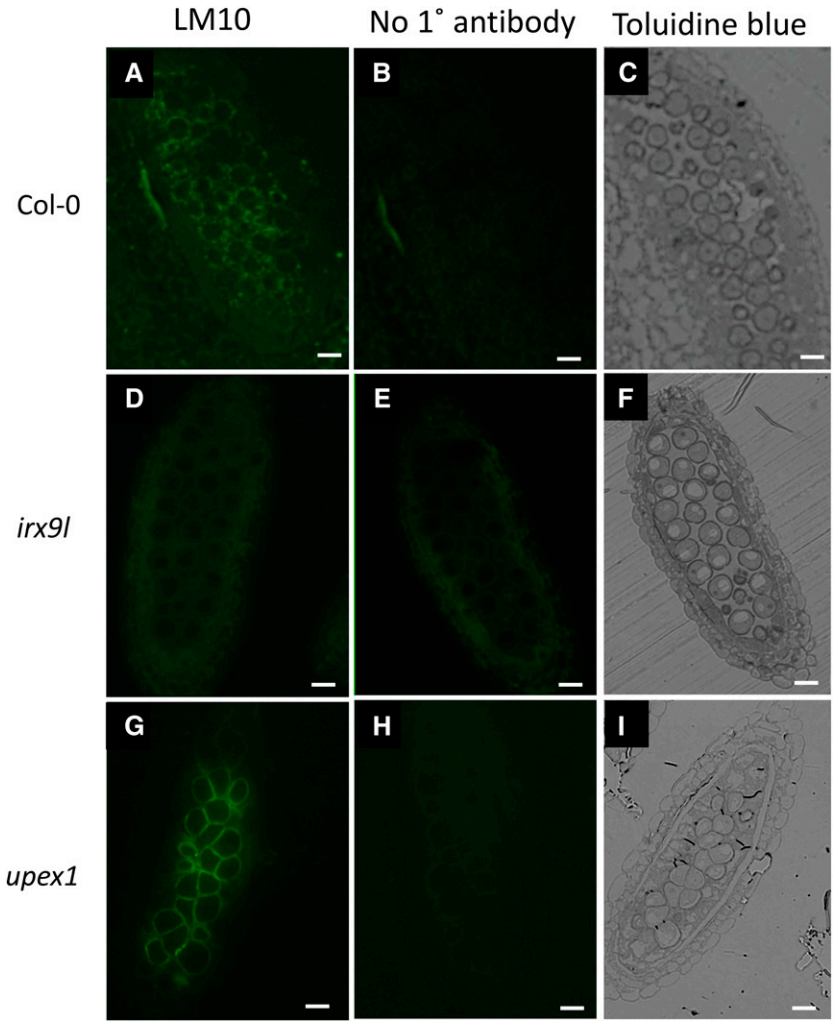

Figure 5. Immunohistochemical localization of xylan localization in microspores at uninucleate ring-vacuolate free microspore stage. Samples were high-pressure frozen and embedded in LR White medium-grade resin, then treated with LM10 antibodies followed by secondary antibodies conjugated with Alexa 488, with secondary antibody alone (no 1° antibody) or stained with toluidine blue to visualize anthers and microspores. A, B, and C, Sections taken from wild-type anthers; D, E, and F, sections taken from *irx9l* anthers; G, H, and I, sections taken from *upex1* anthers. A, D, and G, Sections were treated with xylan-specific LM10 primary antibody and secondary antibody. B, E, and H, Sections were treated with secondary antibody only. C, F, and I, Sections were stained with toluidine blue. Scale bars = 20 μm.

expressed during anther development, *proIRX9L::GUS* transformants were generated. Flower buds from *proIRX9L::GUS* transformants were fixed, sectioned, and stained for GUS activity. This revealed that *IRX9L* is expressed throughout the anther, specifically including in the tapetum and developing microspores, at the tetrad stage of anther development, and in mature tricellular pollen grains (Fig. 11).

Unlike *IRX9L*, *UPEX1* encodes a GT with a highly specific expression pattern in developing flower buds and is highly coexpressed with tapetum-expressed genes involved in sporopollenin biosynthesis (de Azevedo Souza et al., 2009; Kim et al., 2010; Dobritsa et al., 2011). To determine the cell types in which *UPEX1* is expressed in during anther development, *proUPEX1::YFP* transformants were generated. Flower buds from *proUPEX::YFP* transformants were examined by 2P microscopy under excitation of 950 nm (YFP excitation). This revealed strong *UPEX1* promoter activity in the tapetum at the early unicellular microspore stage of anther development with no activity visible in other anther cell types, aside from possible low expression in the microspores (Fig. 11).

Given the observed *UPEX1* and *IRX9L* expression patterns, it was of interest to determine if the loss of *UPEX1* and *IRX9L* expression in the gametophyte or sporophyte is responsible for their observed microspore and pollen phenotypes. We identified *upex1*/+ and *irx9l*/+ heterozygotes in segregating populations and assayed the phenotypes of the pollen released from these anthers by SEM. Supplemental Figure S5 shows that all pollen from *upex1*/+ and *irx9l*/+ heterozygote plants had a wild-type phenotype, despite the fact that a 1:1 segregation of mutant and wild-type genotypes is expected in the haploid pollen. This suggests that both *UPEX1* and *IRX9L* are likely to function in the sporophyte to determine exine structure.

Comparison of Exine Structure in Wild-Type, *irx9l*, *irx14l*, *irx14*, *irx9*, and *irx9l upex* Pollen

In order to further test the hypothesis that xylan is a component of the pollen wall required for proper exine patterning, we examined mutants in other GTs involved in xylan synthesis for their pollen phenotypes.

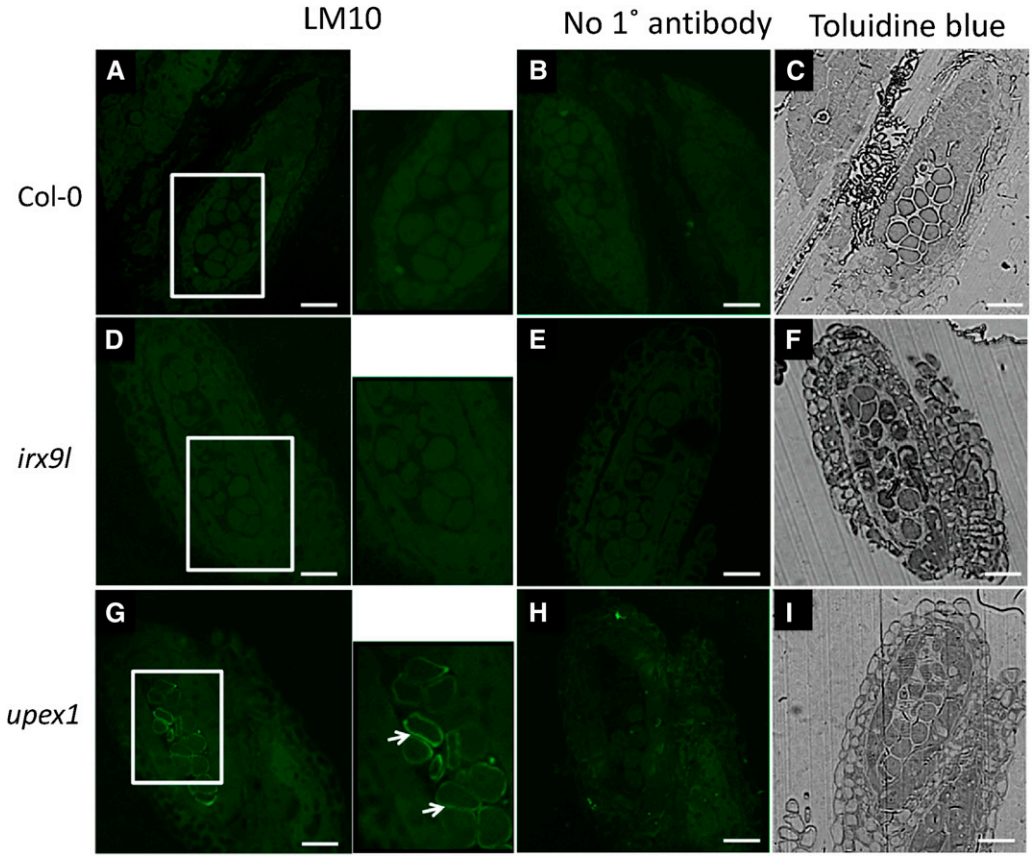

Figure 6. Epifluorescence microscope images of xylan immunolocalization in tetrad stage microspores. Samples were high-pressure frozen and embedded in LR White medium-grade resin, then treated with LM10 antibodies followed by secondary antibodies conjugated with Alexa 488, with secondary antibody alone (no 1° antibody), or stained with toluidine blue to visualize anthers and microspores. A, B, and C, Sections taken from wild-type anthers; D, E, F, sections taken from *irx9l* anthers; G, H, and I, sections taken from *upex1* anthers. A, D, and G, Sections treated with xylan-specific LM10 primary antibody and secondary antibody; B, E, and H, sections treated with secondary antibody only. C, F, and I, Sections stained with toluidine blue. Higher-magnification panels adjacent to A, B, and C represent the areas indicated by the corresponding white boxes. Arrows indicate fluorescence surrounding LM10-treated *upex1* microspores, which were lacking in Col-0 and *irx9l* samples. Bars = 20 μm.

Like *IRX9* and *IRX9L*, *IRX14* and *IRX14L* encode GT family 43 xylosyltransferases, and based on mutant phenotypes, IRX14/IRX14L are proposed to be rate-limiting components of the β-1-4-xylan synthesis machinery (Wu et al., 2010). We obtained *irx9*, *irx14*, and *irx14l* mutants and compared the phenotypes of their mature pollen grains to those of *irx9l* and wild-type using both light microscopy and SEM. Auramine-O-stained pollen grains viewed by fluorescence light microscopy revealed that pollen grains from *irx9* and *irx14* mutants were indistinguishable from wild-type pollen grains (Fig. 12). However, pollen from the *irx14l* mutant had a *spg* exine phenotype similar to *irx9l* (Fig. 12). We also examined the pollen grains from these mutants using SEM. Similar results were obtained, and only pollen from *irx9l* and *irx14l* plants (Fig. 12) had the *spg*, collapsed pollen grain phenotypes previously observed.

Finally, to genetically test the relationship between *UPEX1* and *IRX9L* in exine patterning, we generated *upex1 irx9l* double mutants. Like the single mutants, *upex1 irx9l* double mutants were fertile but exhibited defective exine patterning (Supplemental Fig. S6). Examination of mature pollen grains by Auramine O staining and by SEM suggested that the double mutants have an additive phenotype, with both a *spg* phenotype typical of *irx9l* and a detached exine phenotype typical of *upex1*.

DISCUSSION

Genetic Analysis Reveals Roles for GTs in Primexine Formation, Sporopollenin Deposition, and Exine Patterning

Here, we provide evidence that *IRX9L/SPG* and *UPEX1*, two genes encoding GTs previously identified by Dobritsa et al., (2011) in a large-scale genetic screen for mutants defective in pollen exine patterning, are defective in primexine formation early in microspore development at the stage when free microspores are

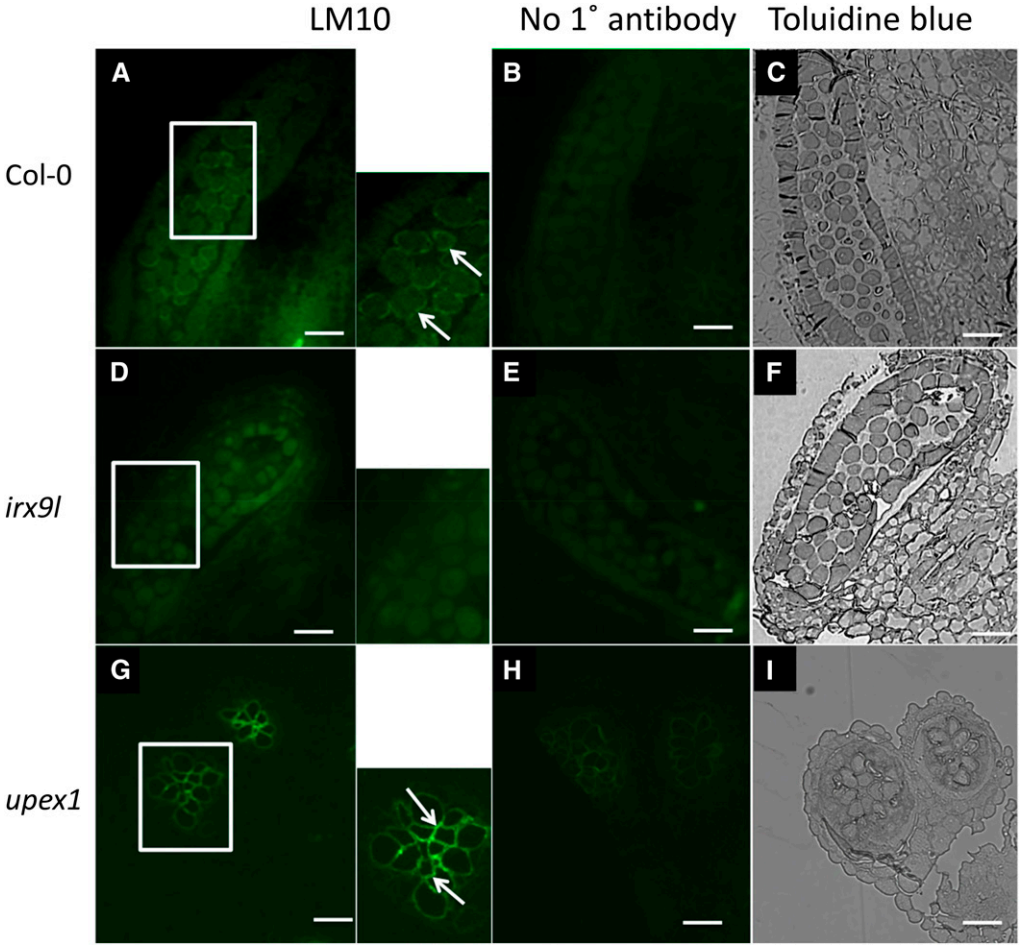

Figure 7. Epifluorescence microscope images of xylan immunolocalization in early unicellular microspore stage microspores. Samples were high-pressure frozen and embedded in LR White medium-grade resin, then treated with LM10 antibodies followed by secondary antibodies conjugated with Alexa 488, with secondary antibody alone (no 1° antibody), or stained with toluidine blue to visualize anthers and microspores. A, B, and C, Sections taken from wild-type anthers; D, E, and F, sections taken from *irx9l* anthers; G, H, and I, sections taken from *upex1* anthers. A, D, and G, Sections treated with xylan-specific LM10 primary antibody and secondary antibody; B, E, and H, sections treated with secondary antibody only. C, F, and I, Sections stained with toluidine blue. Higher-magnification panels adjacent to A, B, and C represent the areas indicated by the corresponding white boxes. Arrows indicate fluorescence surrounding LM10-treated Col-0 and *upex1* microspores, which was lacking in *irx9l* samples. Bars = 20 μm.

released from tetrads and at the time when incipient patterned sporopollenin deposition (probaculae formation) occurs on wild-type microspores (Quilichini et al., 2014a). Furthermore, using the LM10 antibody, we show that the wild-type primexine contains xylan, which was not detected in *irx9l* microspores and was altered in its reactivity to LM10 in *upex1* plants. These data, combined with defects in probacula formation, sporopollenin deposition, and exine patterning observed in *irx9l* and *upex1* mutants, demonstrate that one or more xylan-containing cell wall matrix polysaccharides is required for exine patterning and suggest that proper positioning of probaculae and anchoring of sporopollenin to the surface of microspores at the tetrad stage requires this primexine component. Furthermore, since *UPEX1* encodes a GalT likely involved in AGP galactosylation, our work suggests that one or more AGPs may play a role in primexine structure and could function as a substrate for sporopollenin anchoring to the microspore surface. Our work thus provides a unique and direct link between primexine cell wall biochemistry and sporopollenin deposition and exine patterning.

A recent reanalysis of pollen wall and tapetum development over the course of Arabidopsis anther development that employed TEM coupled with cryofixation to improve preservation of subcellular ultrastructure highlights the tight relationship between appearance of primexine, probacula formation, and sporopollenin deposition at the tetrad stage of microspore development (Quilichini et al., 2014a). This temporal sequence of events and mutants defective both in primexine development and exine patterning provide evidence in

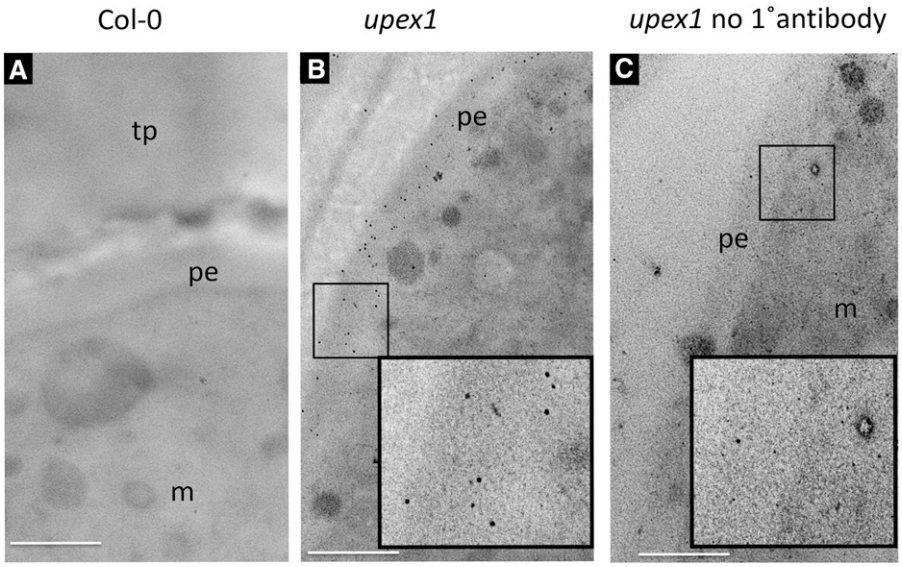

Figure 8. TEM images of xylan immunogold localization in tetrad stage microspores. A, LM10-treated wild-type anther showing immunogold labeling on the primexine layer. B, LM10-treated *upex1* anther showing immunogold labeling on the primexine layer. C, Control *upex1* sample without LM10 treatment. Higher-resolution panels in B and C represent the areas circled by the corresponding white boxes. Gold particles are recognized by their uniform nature and diameters of 10 nm. m, Microspore; pe, primexine; tp, tapetum. Bars = 500 nm.

support of the consensus view that a primary function of the primexine in pollen wall formation is to provide a substrate on the developing microspore for sporopollenin deposition, polymerization, and patterning (Heslop-Harrison, 1968b; Ariizumi and Toriyama, 2011; Quilichini et al., 2015a; Shi et al., 2015). Although chemical staining suggests that primexine contains neutral and acidic polysaccharides and cellulose components (Heslop-Harrison, 1968b) and its formation has been thus assumed to require polysaccharide metabolism (Jiang et al., 2013; Shi et al., 2015), to our knowledge, no further direct biochemical or genetic data has been reported that support this contention, nor are there existing data on the specific nature of the polysaccharide polymers other than cellulose that may contribute to primexine structure and function. Our work now provides new insights into the previously elusive biochemistry of the primexine and links it to key morphological events in pollen wall development, namely sporopollenin anchoring and exine patterning.

Role of Xylan Polysaccharide Primexine

GXs, hemicellulose polymers that are characterized by xylan backbones modified by substitution with α-(1→2)-linked glucuronosyl and 4-*O*-methyl glucuronosyl residues, are major components of dicot secondary cell walls

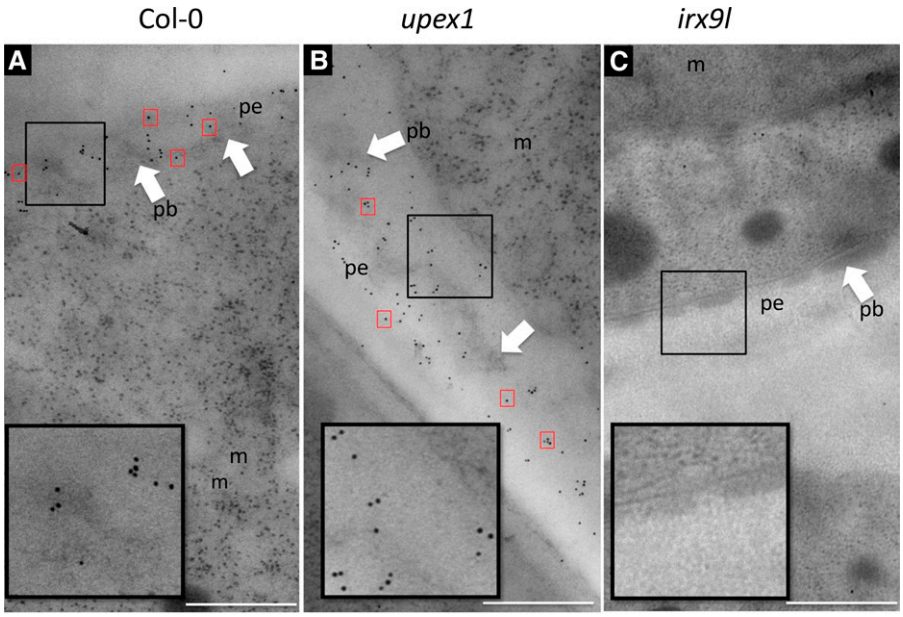

Figure 9. TEM images of xylan immunogold localization in microspores at early uninucleate microspore stage. A and B, LM10-treated wild-type anther. C and D, LM10-treated *upex1* anther showing immunogold labeling surrounding exine. E and F, LM10-treated *irl9l* anther showing the absence of immunogold labeling primexine layer. Higher-resolution panels in B and C represent the areas circled by the corresponding black boxes. Gold particles are recognized by their uniform nature and diameters of 10 nm, which clearly distinguish them from other particles, likely ribosomes, in the microspore cytoplasm. Representative gold particles are boxed by red squares. Arrows indicate incipient probaculae. m, Microspore; pb, probacula; pe, primexine. Bars = 500 nm.

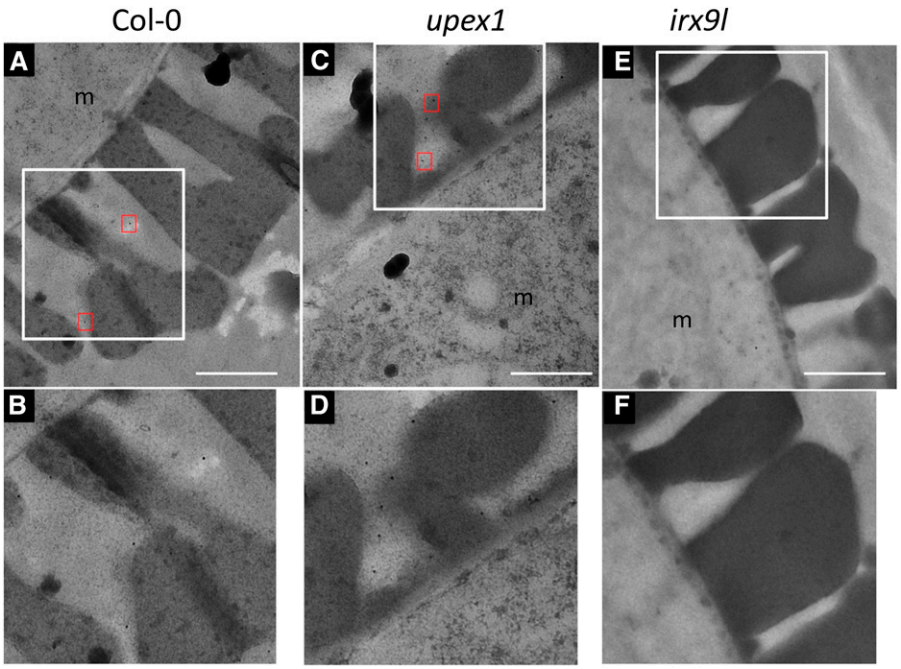

Figure 10. TEM images of xylan immunogold localization in microspores at miduninucleate microspore stage. A, LM10-treated wild-type anther. C, LM10-treated *upex1* anther showing immunogold labeling on the primexine layer. E, LM10-treated *irl9l* anther showing the absence of immunogold labeling layer. Higher-resolution panels in B, D, and F represent the areas circled by the corresponding white boxes in A, C, and E. Gold particles (red boxes) are recognized by their uniform nature and diameters of 10 nm. m, Microspore. Bars = 500 nm.

(Scheller and Ulvskov, 2010). Arabidopsis mutants defective in xylan biosynthesis typically exhibit *irx* phenotypes characterized by collapsed vessel elements (Hao and Mohnen, 2014), which suggests a key role for GX in secondary cell wall structure and function. The *SPG2* locus, identified by its *spg* exine patterning phenotype (Dobritsa et al., 2011) is synonymous to *IRX9L*, which, like *IRX9*, encodes a member of the GT43 family of GTs (Peña et al., 2007; Wu et al., 2010). Similarly, the paralogs *IRX14* and *IRX14L* also encode members of the GT43 family. IRX9 and IRX14 play major, nonredundant roles in xylan backbone elongation required for GX biosynthesis (Hao and Mohnen, 2014), although their presumed functions as xylan:xylosyltransferases with GT enzymatic activity has recently been called into question (Ren et al., 2014). Genetic evidence suggests that *IRX9* and its paralog *IRX9L*, as well as *IRX14* and its paralog *IRX14L*, encode pairs of proteins with the same functions in the biosynthesis of the xylan backbone (Lee et al., 2011; Keppler and Showalter, 2010; Wu et al., 2010). However, the lack of an *irx* phenotype in inflorescence stem vascular bundles in the *irx9l* and *irx14l* mutants suggests that

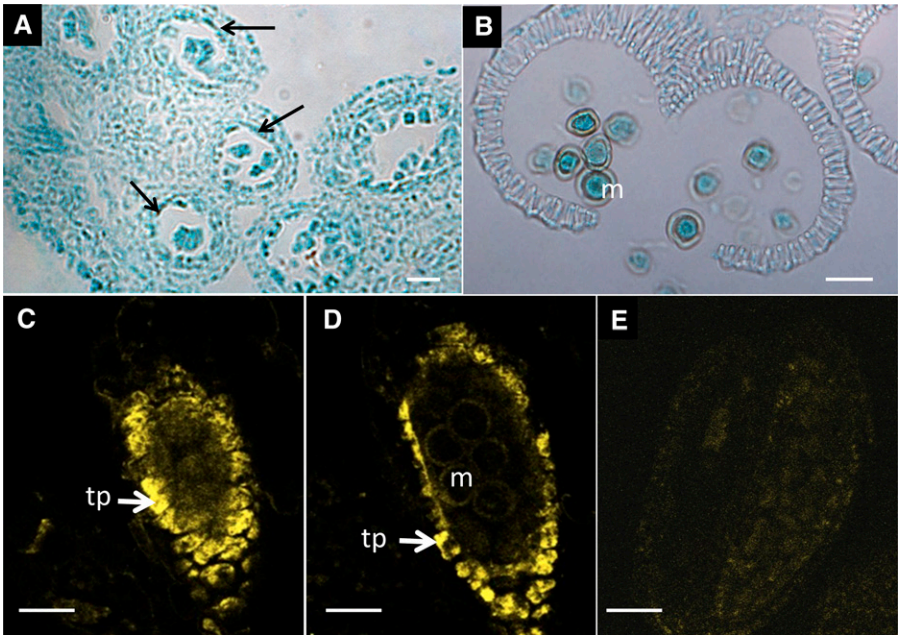

Figure 11. Reporter gene expression patterns directed by *proIRX9L* and *proUPEX1*. A, *proIRX9L:GUS* expression in a tetrad stage anther of a *proIRX9L:GUS* transformant. B, *proIRX9L:GUS* expression in a dehiscent stage anther *proIRX9L:GUS* transformant. C, Longitudinal optical section from near the top of a locule at early unicellular free microspore stage, taken from a *proUPEX:YFP* transformant and imaged by 2P microscopy; fluorescence false colored with yellow. D, Longitudinal optical section from near the middle of the same locule as in C at early unicellular free microspore stage, imaged by 2P microscopy; fluorescence false colored with yellow. E, Control longitudinal optical section of a wild-type anther from near the middle of a locule at early unicellular free microspore stage, imaged by 2P microscopy; fluorescence false colored with yellow. A, Arrows point at tapetum within the anther. tp, Tapetum; m, microspore. A and B, Bars = 25 μm; D, E, and F, bars = 50 μm.

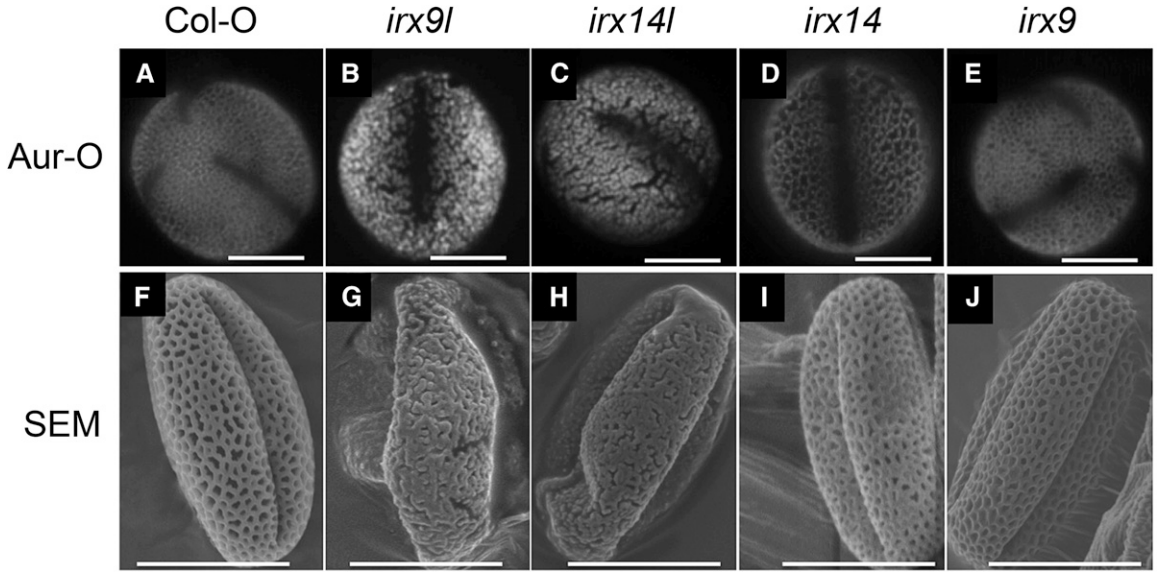

Figure 12. Comparison of exine structure in wild-type, *irx9l*, *irx14l*, *irx14*, and *irx9* pollen. A to E, Confocal micrographs of mature pollen grains taken from the genotypes indicated and stained with the fluorescent dye Auramine O (Aur-O). F to J, SEM micrographs of pollen grains taken from the same genotypes. Pollen from *irx14* and *irx9* mutants were indistinguishable from wild type. *irx14l* shares similar *spg* exine and partially collapsed pollen grain phenotypes with *irx9l*. Bars = 10 μm.

IRX9L and IRX14L play minor roles in secondary wall GX biosynthesis, relative to IRX9 and IRX14 (Wu et al., 2010). The *spg* phenotypes of *irx9l* and *irx14l* pollen grains (Dobritsa et al., 2011; Figs. 1 and 12), together with the defects in primexine and probacula formation of *irx9l* microspores at the tetrad stage (Fig. 4), indicate that IRX9L, and likely IRX14L, play significant roles in xylan biosynthesis during primexine formation in pollen wall development.

The thinner primexine surrounding the *irx9l* microspores revealed by TEM (Fig. 4) could be the result of a defect in a xylan component in the primexine layer whose synthesis requires IRX9L. The presence of LM10 signal in developing wild-type microspores after the tetrad stage and in *upex1* microspores at the tetrad stage and later (Figs. 6, 7, and 8), and the lack of LM10 signal in *irx9l* microspores in all developmental stages (Figs. 5, 6, and 7), suggest that xylan-containing polysaccharides are incorporated into microspore walls, and that this depends on IRX9L function. The lack of LM10 signal in wild-type pollen at the tetrad stage where primexine is first visible (Quilichini et al., 2014a; Figs. 4 and 8) could be due to xylan epitopes being below the detection limit or being masked by other wall components at this stage. Indeed, LM10 staining was detected at the tetrad stage of *upex1* microspores (Fig. 6), and immunogold TEM showed that such epitopes were localized to the primexine in tetrad stage *upex1* microspores (Fig. 9). This suggests greater abundance of xylan in *upex1* primexine and/or greater accessibility of xylan epitopes. The latter possibility is consistent with the altered morphology of the *upex1* primexine (discussed below).

Immunogold TEM showed that xylan-containing epitopes are localized to the primexine of wild-type microspores at the early uninucleate stage when incipient probaculae are present and are absent at this stage in the primexine of *irx9l* microspores (Fig. 9), providing further evidence for xylan in the primexine. At later stages of microspore development, xylan signal was observed in the exine in areas surrounding baculae, possibly from remnant primexine that reported to forming a loose mesh around baculae after microspore release (Quilichini et al., 2014a). Since the less reticulate and shorter baculae of *irx9l* pollen grains are correlated with an altered primexine layer in *irx9l* microspores depleted in xylan, an attractive hypothesis is that xylan-containing polysaccharides in the primexine participate in generating a matrix required for sporopollenin assembly on the microspore surface early in development. Although the biochemical nature of the xylan found in the primexine is unknown, it is of interest that highly branched xylan polysaccharides requiring *IRX14* are involved in anchoring of pectin-containing mucilage of the Arabidopsis seed surface (Voiniciuc et al., 2015).

Potential Role for AGPs in Primexine Structure and Function

The *upex1* mutant shows two striking phenotypes, exine that is irregular and poorly anchored to the microspore surface (Figs. 1, 3, and 4), and a primexine cell wall layer that appears less compact than wild type (Fig. 4) with enhanced staining by the LM10 antibody, suggesting more abundant or more accessible xylan epitopes. Close examination of the primexine with incipient baculae at the late tetrad stage shows uneven and irregular sporopollenin deposition relative to wild

type at this early stage, which is more pronounced at later stages of microspore development (Fig. 4). Based on these observations, UPEX1 appears to be required for structural properties of the primexine wall and proper exine patterning. *UPEX1* encodes a family 31 GT, one of 20 putative GalTs identified in the Arabidopsis genome (Qu et al., 2008), and one of eight GalT genes considered likely to encode β-(1,3)-GalTs that catalyze formation of the β-(1,3)-galactan backbones of AGP *O*-linked glycans, which contribute up to 95% of AGP mass. Indeed, *UPEX1* is closely related to *GALT31A* (At1g32930), which has been demonstrated to elongate β-1,6-galactan side chains in AGPs (Geshi et al., 2013) and is in a sister clade to the Hyp *O*-GalTs HPGT1, HPGT2, and HPGT3 that initiate transfer Gal residues to Hyp residues of AGPs (Ogawa-Ohnishi and Matsubayashi, 2015). Based in these data, it is very likely that *UPEX1* encodes a GalT involved in AGP galactosylation, and recent data show that UPEX1 indeed has GalT activity capable of AGP galactosylation (J. Narisco and T. Bacic, personal communication).

Since, according to the BAR eFP browser (Winter et al., 2007; http://bar.utoronto.ca), *UPEX1* has a very restricted pattern of expression in young flower buds at the time of microspore development, is highly coexpressed with *ACOS5* and other genes required for sporopollenin biosynthesis (de Azevedo Souza et al., 2009), and shows a tapetum-specific expression pattern (Fig. 11), UPEX1 may play a specialized role in AGP galactosylation during microspore development, consistent with a role for AGPs in primexine structure and function. Furthermore, AGPs have been reported in the walls of developing microspores at the tetrad and later-stage anthers in Arabidopsis at the time of primexine development, as well as in the tapetum, and were hypothesized to be secreted from the tapetal cells (Coimbra and Pereira, 2012).

Interestingly, *AGP6* expression in tapetal cells has been shown to be critical for the formation of the nexine, the innermost specialized layer of the exine that is required for pollen grain wall integrity (Jia et al., 2015). Expression of *AGP6*, *AGP11*, *AGP23*, and *AGP43* is dramatically reduced in the *transposable element silencing via AT-Hook* mutant defective in nexine formation (Jia et al., 2015). These data provide additional support for potentially important structural roles for AGPs in both the nexine and primexine microspore cell wall layers. Consistent with our data, recent findings indicate the presence UPEX1-dependent AGP epitopes in the microspore wall at the early free microspore stage (J. Narisco and T. Bacic, personal communication). While further work is required to test for localization of AGPs dependent on UPEX1 activity in the primexine, these data are consistent with a model in which both AGPs and xylan components of the primexine wall contribute to the deposition of sporopollenin to the microspore surface in a regular pattern, as well as to its anchoring to the microspore surface. However, the apparent additive phenotype of *irx9l upex1* double mutants, with features of both single mutants in mature pollen grains, suggests that exine adherence and patterning may be meditated by distinct processes.

Recently, covalent attachment between an AGP (APAP1) and pectic and arabinoxylan cell wall matrix polysaccharides been demonstrated in Arabidopsis cell walls and proposed to be an important structural feature of plant cell walls (Tan et al., 2013). Glycome profiling revealed that pectin and xylan epitopes are significantly more extractable from *apap1* mutant cell walls than wild-type walls, suggesting a less structured wall in the absence of APAP1 (Tan et al., 2013). We find parallels to the findings of Tan et al. (2013) in *upex1* primexine, which appears morphologically more diffuse and in which xylan epitopes are more readily detected. This suggests that analogous covalent interactions between AGPs and xylan-containing polysaccharides could play a role in the structure of the primexine wall and in its function as a substrate for initial sporopollenin deposition.

Sporophytic Functions of *IRX9L* and *UPEX1*

Previous genetic analyses suggest that primexine formation requires sporophytic functions, since all pollen produced by plants heterozygous for primexine-defective mutants (e.g. *rpg1*/+, *dex1*/+1, and *nef1*/+) appears wild type-like (Ariizumi and Toriyama, 2011). Similarly, we found that all pollen from *irx9l*/+ and *upex1*/+ heterozygotes had wild-type exine phenotypes (Supplemental Fig. S5). Furthermore, *proUPEX1::YFP* is expressed primarily in the tapetum with possible weak expression in microspores, consistent with in situ hybridization data (Peiffer et al., 2008), and *proIRX9L::GUS* is expressed in all or most anther cell types, including the tapetum (Fig. 12). Taken together, these data suggest that the biochemical functions of IRX9L and UPEX1 in sporophytic tapetal cells may be sufficient for xylan and AGP deposition in the surface primexine of haploid microspores that lack these proteins, even at a stage when they are surrounded by a callose wall. Further work on the localization of the respective enzymes, and the potential trafficking of xylan and glycosylated AGPs from the tapetum, will be required to resolve this question.

MATERIALS AND METHODS

Plant Material and Growth Conditions

Seeds were sterilized with 70% ethanol and put through a cold treatment of 2 d at 4°C. Seeds were then placed at 20°C under 24-h fluorescent lighting for germination. Ten to fourteen days later, the seedlings were grown in a 21°C chamber under long-day conditions (16 h light/8 h dark).

Arabidopsis (*Arabidopsis thaliana*) T-DNA insertion mutants SAIL_544_C02 and SALK_091466 for *UPEX1* (At1g33430) and Salk_037323 for *IRX9L* were identified using The Arabidopsis Information Resource (http://www.arabidopsis.org) and ordered from the Arabidopsis Biological Resource Center (Alonso et al., 2003; http://www.abrc.osu.edu). Homozygous plants were identified by PCR using genomic DNA with gene-specific primers that anneal to 5′ and 3′ to the insertion site and insert specific primers (Supplemental Table S2). *irx9l upex1* double mutants were identified in an F2 population derived from a cross between homozygous *irx9l* and *upex1* lines, using the same primers.

RNA Isolation and RT-PCR

Different Arabidopsis tissues (70 mg) were isolated and frozen in liquid nitrogen before grinding to a fine powder using beads (1.0 mm zirconia/silica; BioSpec) with a beater at 4°C at a speed of 6000 rpm (Bertin Precellys 24). RNA was extracted with TRIzol (Invitrogen) and cleaned with a DNAse Kit (Invitrogen). cDNA was generated using Superscript II Reverse Transcriptase (Invitrogen) following the manufacturer's protocol. Variant specific primers were used to detect which *UPEX1* splice variants is the dominant form. The PCR conditions used to amplify the corresponding cDNA sequences were 95°C for 3 min, followed by 29 cycles of 94°C for 30 s, 55°C for 30 s, 72°C for 60 s, and ending with 72°C for 10 min, using Bio-Rad Master Q mix in a 10 μL total reaction.

Fluorescence Microscopy

Pollen was stained with 0.01% Auramine O in water for 3 min. Samples were rinsed with water before being mounted in water and secured with a thickness number 1.5 coverslip (Fisher Scientific). Pollen was examined with UltraView Vox (PerkinElmer) spinning disk confocal mounted on a Leica DM16000 inverted microscope and a Hamamatsu 9100-02 CCD camera. Excitation/emission filters GFP (488/525) was used along with Leica oil immersion 63× objective (plan-Apo, NA 1.4). Velocity image analysis software (Improvision) was used to process all images taken with this microscopy.

2P Laser Scanning Microscopy Analysis

Individual anthers were immersed in a drop of water and sealed beneath a thickness number 1.5 coverslip (Fisher Scientific) in a small petri plate. Intrinsic fluorescence of live anther tissues was imaged using an Olympus Multiphoton Laser Scanning Microscope FV1000MPE connected to a Mai Tai Deepsee laser using an excitation wavelength at 640 nm. The objective used was Olympus XLPLN 25× WMP with NA 1.05. Images were captured with Olympus Fluoview version 3.1.

SEM

Pollen was collected from open flowers and placed on sticky tabs on aluminum SEM stubs (Ted Pella). Samples were coated with 9 nm gold-platinum with a Cressington 208HR high-resolution sputter coater. Samples were examined with a Hitachi S-2600N variable pressure SEM.

Sample Preparation for Microscopy

Formaldehyde-acetic acid-ethanol fixation was carried out described by Kim et al. (2010). Samples were dehydrated using a series of 75%:25%, 50%:50%, 25%:75% ethanol:Safeclear solutions (Fisher Scientific, Protocol). Following the two washes with 100% Safeclear, samples were treated with 25%:75% paraffin (Paraplast plus; Sigma):Safeclear in a 60°C for 4 h. Paraffin:Safeclear (50%:50%) was then used to replace the previous solution, and samples were kept at 60°C overnight. Fresh molten 100% paraffin was used to replace the paraffin Safeclear solution four times at 60°C every 12 h. Embedded samples were sectioned with a microtome (Microm HM325) to 10 μm thickness. Sections were placed on a water drop on poly-L-Lys-coated slides (Electron Microscopy Science) and dried at 40°C for 2 to 3 h.

For high-pressure freezing and freeze substitution of samples, we used the protocol described by McFarlane et al. (2008). Infiltration with LR White (EM.co medium hard grade) was performed according to the protocol of Spurr (1969). For Spurr's epoxy resin sample preparation, the same protocols were used as the LR White samples, except the freeze substitution medium contained 2% osmium tetroxide in HPLC grade acetone with 8% (v/v) dimethoxypropane. Spurr's resin (Canemco) was carried out according to McFarlane et al. (2008) and Spurr (1969). Resin-embedded samples were transferred to capsules (BEEM embedding capsules no. 70020; Electron Microscopy Sciences) and left at 60°C overnight for polymerization.

TEM

The protocol used was described by McFarlane et al. (2008). Samples were imaged using a Hitachi H7600 TEM connected with an AMT Advantage (1 megapixel) CCD camera (Advanced Microscope Technologies).

Immunolabeling

For immunofluorescence imaging, LR White samples were sectioned to 0.35 μm thickness using a Reichert Ultracut E ultramicrotome and put on to Teflon-coated slides. Immunolabeling for fluorescence light microcopy using a semithin section protocol was described by McFarlane et al. (2008). The primary antibody LM10 against xylan epitopes (McCartney et al., 2005; a gift of Dr. A. Lacey Samuels, University of British Columbia) was used at a 1:100 dilution, followed by 1:100 dilution of the secondary antibody (rabbit anti-rat-Alexa 488). Sections were imaged using Zeiss Axioplan2 microscope connected to Q-cam digital camera with excitation/emission GFP filter (470/525).

For immunogold imaging, LR White sample sections with a thickness of 60 nm to 75 nm were sectioned using a Reichert Ultracut E ultramicrotome and placed on 100 mesh nickel grids coated with formvar. Immunogold labeling for TEM on ultrathin sections was performed as described by McFarlane et al. (2008). The primary antibody LM10 was used at a dilution of 1:20, followed by the secondary antibody 10 nm gold-conjugated goat anti-rat at 1:50 dilution (Ted Pella). Staining and imaging LR White samples are the same as staining and imaging Spurr samples.

Cloning and Plant Transformation

To generate *proIRX9L:GUS*, a 1244-bp Arabidopsis genomic DNA fragment with 1174 bp 5′ to the translation start site was subcloned into pCR8/GW/TOPO (Invitrogen) following the manufacturer's protocol. The DNA was then subcloned into pEarlyGate101 Gateway binary vector (Nakagawa et al., 2007). To generate *proUPEX:GUS* and *proUPEX::YFP*, a 1030-bp Arabidopsis genomic DNA fragment with 1022 bp 5′ to the translation start site was subcloned into pCR8/GW/TOPO (Invitrogen) using the methods described above. The pGWB3 binary vector was used as the destination vector for the next transformation to generate *proUPEX:GUS*, while the PGWB4 binary vector was used as the other destination vector for the transformation to generate *proUPEX::YPF*. T-DNA vectors were transformed into electrocompetent *Agrobacterium tumefaciens* strain GV3101 and transformation into wild-type plants was performed using the floral-dip method (Clough and Bent, 1998).

GUS Assay

The protocol used was as described by de Azevedo Souza et al. (2009), using flower buds immersed in the GUS substrate solution (50 nM sodium phosphate buffer, pH 7.0, 0.1% Triton X-100, 3 mM potassium ferricyanide, 3 mM potassium ferrocyanide, and 1 mM 5-bromo-4-chloro-3-indolyl β-D-glucuronide). Following 2 h of vacuum infiltration, samples were incubated at 37°C overnight in the dark.

Accession Numbers

Sequence data from this article can be found in the GenBank/EMBL data libraries under accession numbers *IRX9L*, At1g27600; *IRX14L*, At5g67230; and *UPEX1*, At1g33430.

Supplemental Data

The following supplemental materials are available online.

Supplemental Figure S1. Characterization of the *irx9l-1* mutant.

Supplemental Figure S2. *UPEX* gene structure and expression.

Supplemental Figure S3. *UPEX1.1* is the major variant expressed in plants and *upex* has normal vegetative growth.

Supplemental Figure S4. Quantification of LM10 immunogold signal in wild-type, *upex1*, and *irx9l* microspore walls.

Supplemental Figure S5. Scanning electron micrographs of pollen derived from *upex1/UPEX1* and *irx9l IRX9L* plants.

Supplemental Figure S6. Comparison of exine structure in wild-type, *irx9l*, *upex1*, and *irx9l upex1* pollen.

Supplemental Table S1. Fertility of *irx91* and *upex1* mutants.

Supplemental Table S2. List of primers used for cloning, RT-PCR, and genotyping Arabidopsis mutant lines.

ACKNOWLEDGMENTS

We thank the Arabidopsis Biological Resource Center (The Ohio State University) and The Arabidopsis Information Resource for information and genetic resources. We gratefully acknowledge the support of the University of British Columbia Bioimaging Facility and thank Etienne Grienenberger (University of California, Berkeley) and Teagen Quilichini (University of British Columbia) for advice and discussions. We thank Wei Zeng and Tony Bacic (University of Melbourne) for sharing data on UPEX1 function prior to publication.

Received March 24, 2016; accepted July 30, 2016; published August 5, 2016.

LITERATURE CITED

Ahlers F, Bubert H, Steuernagel S, Wiermann R (2000) The nature of oxygen in sporopollenin from the pollen of Typha angustifolia L. Z Naturforsch C **55:** 129–136

Ahlers F, Lambert J, Wiermann R (2003) Acetylation and silylation of piperidine solubilized sporopollenin from pollen of Typha angustifolia L. Z Naturforsch C **58:** 807–811

Alonso JM, Stepanova AN, Leisse TJ, Kim CJ, Chen H, Shinn P, Stevenson DK, Zimmerman J, Barajas P, Cheuk R, et al (2003) Genome-wide insertional mutagenesis of Arabidopsis thaliana. Science **301:** 653–657

Ariizumi T, Hatakeyama K, Hinata K, Inatsugi R, Nishida I, Sato S, Kato T, Tabata S, Toriyama K (2004) Disruption of the novel plant protein NEF1 affects lipid accumulation in the plastids of the tapetum and exine formation of pollen, resulting in male sterility in Arabidopsis thaliana. Plant J **39:** 170–181

Ariizumi T, Toriyama K (2011) Genetic regulation of sporopollenin synthesis and pollen exine development. Annu Rev Plant Biol **62:** 437–460

Blackmore S, Wortley AH, Skvarla JJ, Rowley JR (2007) Pollen wall development in flowering plants. New Phytol **174:** 483–498

Blokker P, Boelen P, Broekman R, Rozema J (2006) The occurrence of p-coumaric acid and ferulic acid in fossil plant materials and their use as UV-proxy. Plant Ecol **182:** 197–207

Bubert H, Lambert J, Steuernagel S, Ahlers F, Wiermann R (2002) Continuous decomposition of sporopollenin from pollen of Typha angustifolia L. by acidic methanolysis. Z Naturforsch C **57:** 1035–1041

Campbell JA, Davies GJ, Bulone V, Henrissat B (1997) A classification of nucleotide-diphospho-sugar glycosyltransferases based on amino acid sequence similarities. Biochem J **326:** 929–939

Clough SJ, Bent AF (1998) Floral dip: a simplified method for Agrobacterium-mediated transformation of Arabidopsis thaliana. Plant J **16:** 735–743

Coimbra S, Pereira LG (2012) Arabinogalactan proteins in Arabidopsis thaliana pollen development. *In* YO Çiftçi, ed, Transgenic Plants—Advances and Limitations. InTech Europe, Rijeka, Croatia, pp 329–335

de Azevedo Souza C, Kim SS, Koch S, Kienow L, Schneider K, McKim SM, Haughn GW, Kombrink E, Douglas CJ (2009) A novel fatty Acyl-CoA Synthetase is required for pollen development and sporopollenin biosynthesis in Arabidopsis. Plant Cell **21:** 507–525

Dobritsa AA, Lei Z, Nishikawa S, Urbanczyk-Wochniak E, Huhman DV, Preuss D, Sumner LW (2010) LAP5 and LAP6 encode anther-specific proteins with similarity to chalcone synthase essential for pollen exine development in Arabidopsis. Plant Physiol **153:** 937–955

Dobritsa AA, Geanconteri A, Shrestha J, Carlson A, Kooyers N, Coerper D, Urbanczyk-Wochniak E, Bench BJ, Sumner LW, Swanson R, et al (2011) A large-scale genetic screen in Arabidopsis to identify genes involved in pollen exine production. Plant Physiol **157:** 947–970

Dobritsa AA, Shrestha J, Morant M, Pinot F, Matsuno M, Swanson R, Møller BL, Preuss D (2009) CYP704B1 is a long-chain fatty acid ω-hydroxylase essential for sporopollenin synthesis in pollen of Arabidopsis. Plant Physiol **151:** 574–589

Geshi N, Johansen JN, Dilokpimol A, Rolland A, Belcram K, Verger S, Kotake T, Tsumuraya Y, Kaneko S, Tryfona T, et al (2013) A galactosyltransferase acting on arabinogalactan protein glycans is essential for embryo development in Arabidopsis. Plant J **76:** 128–137

Grienenberger E, Kim SS, Lallemand B, Geoffroy P, Heintz D, Souza CdeA, Heitz T, Douglas CJ, Legrand M (2010) Analysis of TETRAKETIDE α-PYRONE REDUCTASE function in Arabidopsis thaliana reveals a previously unknown, but conserved, biochemical pathway in sporopollenin monomer biosynthesis. Plant Cell **22:** 4067–4083

Guan YF, Huang XY, Zhu J, Gao JF, Zhang HX, Yang ZN (2008) RUPTURED POLLEN GRAIN1, a member of the MtN3/saliva gene family, is crucial for exine pattern formation and cell integrity of microspores in Arabidopsis. Plant Physiol **147:** 852–863

Hao Z, Mohnen D (2014) A review of xylan and lignin biosynthesis: foundation for studying Arabidopsis irregular xylem mutants with pleiotropic phenotypes. Crit Rev Biochem Mol Biol **49:** 212–241

Heslop-Harrison J (1968a) Pollen wall development. The succession of events in the growth of intricately patterned pollen walls is described and discussed. Science **161:** 230–237

Heslop-Harrison J (1968b) Wall development within the microspore tetrad of *Lilium longiflorum*. Can J Bot **46:** 1185–1192

Jia QS, Zhu J, Xu XF, Lou Y, Zhang ZL, Zhang ZP, Yang ZN (2015) Arabidopsis AT-hook protein TEK positively regulates the expression of arabinogalactan proteins for Nexine formation. Mol Plant **8:** 251–260

Jiang J, Zhang Z, Cao J (2013) Pollen wall development: the associated enzymes and metabolic pathways. Plant Biol (Stuttg) **15:** 249–263

Keppler BD, Showalter AM (2010) IRX14 and IRX14-LIKE, two glycosyl transferases involved in glucuronoxylan biosynthesis and drought tolerance in Arabidopsis. Mol Plant **3:** 834–841

Kim SS, Grienenberger E, Lallemand B, Colpitts CC, Kim SY, de Azevedo Souza C, Geoffroy P, Heintz D, Krahn D, Kaiser M, et al (2010) LAP6/POLYKETIDE SYNTHASE A and LAP5/POLYKETIDE SYNTHASE B encode hydroxyalkyl α-pyrone synthases required for pollen development and sporopollenin biosynthesis in Arabidopsis thaliana. Plant Cell **22:** 4045–4066

Lallemand B, Erhardt M, Heitz T, Legrand M (2013) Sporopollenin biosynthetic enzymes interact and constitute a metabolon localized to the endoplasmic reticulum of tapetum cells. Plant Physiol **162:** 616–625

Lee C, Teng Q, Zhong R, Ye Z-H (2011) Molecular dissection of xylan biosynthesis during wood formation in poplar. Mol Plant **4:** 730–747

McCartney L, Marcus SE, Knox JP (2005) Monoclonal antibodies to plant cell wall xylans and arabinoxylans. J Histochem Cytochem **53:** 543–546

McFarlane HE, Young RE, Wasteneys GO, Samuels AL (2008) Cortical microtubules mark the mucilage secretion domain of the plasma membrane in Arabidopsis seed coat cells. Planta **227:** 1363–1375

Morant M, Jørgensen K, Schaller H, Pinot F, Møller BL, Werck-Reichhart D, Bak S (2007) CYP703 is an ancient cytochrome P450 in land plants catalyzing in-chain hydroxylation of lauric acid to provide building blocks for sporopollenin synthesis in pollen. Plant Cell **19:** 1473–1487

Nakagawa T, Kurose T, Hino T, Tanaka K, Kawamukai M, Niwa Y, Toyooka K, Matsuoka K, Jinbo T, Kimura T (2007) Development of series of gateway binary vectors, pGWBs, for realizing efficient construction of fusion genes for plant transformation. J Biosci Bioeng **104:** 34–41

Ogawa-Ohnishi M, Matsubayashi Y (2015) Identification of three potent hydroxyproline O-galactosyltransferases in Arabidopsis. Plant J **81:** 736–746

Paxson-Sowders DM, Dodrill CH, Owen HA, Makaroff CA (2001) DEX1, a novel plant protein, is required for exine pattern formation during pollen development in Arabidopsis. Plant Physiol **127:** 1739–1749

Peña MJ, Zhong R, Zhou GK, Richardson EA, O'Neill MA, Darvill AG, York WS, Ye ZH (2007) Arabidopsis irregular xylem8 and irregular xylem9: implications for the complexity of glucuronoxylan biosynthesis. Plant Cell **19:** 549–563

Peiffer JA, Kaushik S, Sakai H, Arteaga-Vazquez M, Sanchez-Leon N, Ghazal H, Vielle-Calzada JP, Meyers BC (2008) A spatial dissection of the Arabidopsis floral transcriptome by MPSS. BMC Plant Biol **8:** 43

Qu Y, Egelund J, Gilson PR, Houghton F, Gleeson PA, Schultz CJ, Bacic A (2008) Identification of a novel group of putative Arabidopsis thaliana β-(1,3)-galactosyltransferases. Plant Mol Biol **68:** 43–59

Quilichini TD, Douglas CJ, Samuels AL (2014a) New views of tapetum ultrastructure and pollen exine development in Arabidopsis thaliana. Ann Bot (Lond) **114:** 1189–1201

Quilichini TD, Friedmann MC, Samuels AL, Douglas CJ (2010) ATP-binding cassette transporter G26 is required for male fertility and pollen exine formation in Arabidopsis. Plant Physiol **154:** 678–690

Quilichini TD, Grienenberger E, Douglas CJ (2015a) The biosynthesis, composition and assembly of the outer pollen wall: A tough case to crack. Phytochemistry **113:** 170–182

Quilichini TD, Samuels AL, Douglas CJ (2014b) ABCG26-mediated polyketide trafficking and hydroxycinnamoyl spermidines contribute to pollen wall exine formation in Arabidopsis. Plant Cell **26:** 4483–4498

Quilichini TD, Samuels AL, Douglas CJ (2015b) Analysis of developing pollen grains within intact Arabidopsis thaliana anthers by Olympus two-photon laser scanning microscopy. Bio Protoc **5:** e1677

Ren Y, Hansen SF, Ebert B, Lau J, Scheller HV (2014) Site-directed mutagenesis of IRX9, IRX9L and IRX14 proteins involved in xylan biosynthesis: glycosyltransferase activity is not required for IRX9 function in Arabidopsis. PLoS One **9:** e105014–e105019

Sanders PM, Bui AQ, Weterings K, McIntire KN, Hsu Y-C, Lee PY, Truong MT, Beals TP, Goldberg RB (1999) Anther developmental defects in Arabidopsis thaliana male-sterile mutants. Sex Plant Reprod **11:** 297–322

Scheller HV, Ulvskov P (2010) Hemicelluloses. Annu Rev Plant Biol **61:** 263–289

Scott RJ, Spielman M, Dickinson HG (2004) Stamen structure and function. Plant Cell (Suppl) **16:** S46–S60

Shi J, Cui M, Yang L, Kim Y-J, Zhang D (2015) Genetic and biochemical mechanisms of pollen wall development. Trends Plant Sci **20:** 741–753

Spurr AR (1969) A low-viscosity epoxy resin embedding medium for electron microscopy. J Ultrastruct Res **26:** 31–43

Sun MX, Huang XY, Yang J, Guan YF, Yang ZN (2013) Arabidopsis RPG1 is important for primexine deposition and functions redundantly with RPG2 for plant fertility at the late reproductive stage. Plant Reprod **26:** 83–91

Tan L, Eberhard S, Pattathil S, Warder C, Glushka J, Yuan C, Hao Z, Zhu X, Avci U, Miller JS, et al (2013) An Arabidopsis cell wall proteoglycan consists of pectin and arabinoxylan covalently linked to an arabinogalactan protein. Plant Cell **25:** 270–287

Voiniciuc C, Günl M, Schmidt MH-W, Usadel B (2015) Highly branched xylan made by IRREGULAR XYLEM14 and MUCILAGE-RELATED21 links mucilage to Arabidopsis seeds. Plant Physiol **169:** 2481–2495

Winter D, Vinegar B, Nahal H, Ammar R, Wilson GV, Provart NJ (2007) An "Electronic Fluorescent Pictograph" browser for exploring and analyzing large-scale biological data sets. PLoS One **2:** e718

Wu AM, Hörnblad E, Voxeur A, Gerber L, Rihouey C, Lerouge P, Marchant A (2010) Analysis of the Arabidopsis IRX9/IRX9-L and IRX14/IRX14-L pairs of glycosyltransferase genes reveals critical contributions to biosynthesis of the hemicellulose glucuronoxylan. Plant Physiol **153:** 542–554